analytical chemistry

Article

pubs.acs.org/ac

Ultrasensitive Vapor Detection with Surface-Enhanced Raman Scattering-Active Gold Nanoparticle Immobilized Flow-Through Multihole Capillaries

Maung Kyaw Khaing Oo,[†] Yunbo Guo,[†] Karthik Reddy,[†,‡] Jing Liu,[†] and Xudong Fan*[,†]

[†]Department of Biomedical Engineering and [‡]Department of Electrical Engineering and Computer Science, University of Michigan, Ann Arbor, Michigan 48109, United States

Supporting Information

ABSTRACT: We developed novel flow-through surface-enhanced Raman scattering (SERS) platforms using gold nanoparticle (Au-NP) immobilized multihole capillaries for rapid and sensitive vapor detection. The multihole capillaries consisting of thousands of micrometer-sized flow-through channels provide many unique characteristics for vapor detection. Most importantly, its three-dimensional SERS-active micro-/nanostructures make available multilayered assembly of Au-NPs, which greatly increase SERS-active surface area within a focal volume of excitation and collection, thus improving the detection sensitivity. In addition, the multihole capillary's inherent longitudinal channels offer rapid and convenient vapor delivery, yet its micrometer-sized holes increase the interaction between vapor molecules and SERS-active substrate. Experimentally, rapid pyridine vapor detection (within 1 s of exposure) and ultrasensitive 4-nitrophenol vapor detection (at a sub-ppb level) were successfully achieved in open air at room temperature. Such an ultrasensitive SERS platform enabled, for the first time, the investigation of both pyridine and 4-nitrophenol vapor adsorption isotherms at very low concentrations. Type I and type V behaviors of the International Union of Pure and Applied Chemistry isotherm were well observed, respectively.

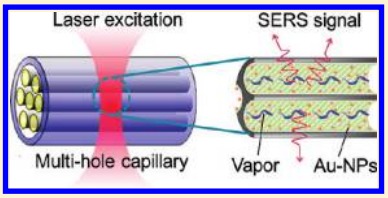

Surface-enhanced Raman scattering (SERS), as a high-sensitivity and high-specificity analytical technique, has been employed in the development of rapid and sensitive analyzers for trace quantity chemical vapor detections to utilize in environmental protection/monitoring, homeland security, and battlefield.[1−9] SERS has the ability to identify chemical molecules and monitor molecular structural changes at extremely low concentrations, even at the single-molecule level.[10−13] In addition, the SERS efficiency can be maximized by tuning nanostructures such as morphologies[8,14,15] and materials.[16] Thus, SERS-based detection possesses great potential in developing simple, sensitive, fast, inexpensive, and robust methods to monitor single or multiple contaminants.[17,18]

However, in vapor-phase detection using SERS, there exists only limited knowledge, as compared to the broadly investigated field of SERS in liquid phase. In the past decade, only a handful of research studies in SERS have been conducted in the context of hazardous gas analysis[1−6] and explosive constituent detection.[7−9] For example, the Vo-Dinh group developed vapor dosimeters using SERS-active nanotextured silver without[1] and with[3] poly(vinylpyrrolidone) coating. They also demonstrated the detection of vapor-phase chemical nerve agent simulants, dimethyl methylphosphonate and diisopropyl methylphosphonate using roughened silver oxide substrates in a closed chamber after several exposure time periods (0−40 min).[2] The Van Duyne group achieved 6 ppm-s of detection limit time for benzenethiol gas phase using a silver film over a nanosphere (AgFON) substrate at a temperature of 356 K.[5] Rae and Khan reported detection of 1% of CO and 1% of N_2O using AgPd substrate.[6] Hill et al. demonstrated detection of vapor exhaled from rubber with Al_2O_3 particles coated with Ag substrate.[4] In the explosive constituent detection, detection limits of 0.4 ag,[8] 5 ppb,[7] and 10 ppt[9] for 2,4-dinitrotoluene vapor were achieved using gold nanoparticle (Au-NP) immobilized substrate, roughened gold foil, and Au-NP cluster arrays, respectively. In addition, off-line and online SERS detectors in conjunction with gas chromatography were also reported.[19−21] However, all these reported SERS substrates are essentially two-dimensional (2-D) nanostructures, which have limited SERS-active surface area within the detection volume and thus restrict their performance in rapid and ultrasensitive vapor detection. Moreover, these substrates do not have readily available flow channels, and they are usually required to be embedded in a stream of vapor flow or placed in a vapor chamber for detection, which is laborious and not efficient. Therefore, it is very attractive to develop a three-dimensional (3-D) SERS platform with efficient fluidics for vapor detection.

In this paper, we present novel flow-through SERS platforms using Au-NP immobilized multihole capillaries for rapid and sensitive vapor detection. The unique configuration provides not only 3-D structures to accommodate much more available SERS-active sites interacting with vapor molecules and to enhance the Raman signal significantly but also well-defined flow-through micrometer-sized channels for convenient analyte delivery and efficient analyte capture. To explore the proposed

Received: January 17, 2012
Accepted: March 7, 2012
Published: March 7, 2012

   dx.doi.org/10.1021/ac300175v | *Anal. Chem.* 2012, 84, 3376−3381

SERS platform's capability, both high vapor pressure (pyridine) and low vapor pressure (4-nitrophenol) gas molecules were employed as model analytes and were investigated in open air space at room temperature. Moreover, the performance of the 3-D multihole capillaries with different inner hole sizes were explored and compared to a single-hole capillary (considered a 2-D structure with a flow channel). The relationship between the SERS intensity and the vapor flow rates of the single-hole and multihole capillaries were also evaluated. Furthermore, we measured the vapor adsorption isotherm, which is essential to explore the nature of the interaction between the gas molecule and the SERS-active substrate. However, measurement of the vapor adsorption isotherm at very low concentrations is very challenging, which is one of the reasons that most of the previous studies using 2-D SERS substrates exhibited only qualitative analysis of vapors. Only with the ultrasensitive SERS platform that we developed here did it become possible to evaluate the behavior of both pyridine and 4-nitrophenol vapor adsorption isotherms for the first time.

EXPERIMENTAL SECTION

Materials. Pyridine (≥99.9%), 4-nitrophenol (PESTANAL, analytical standard), gold(III) chloride solution (30 wt % of $HAuCl_4$ in dilute HCl), poly(allyamine hydrochloride) (PAH) (average molecular weight of 15 000 g/mol), and sulfuric acid (96.0%, Acros Organics, ACS reagent) were purchased from Sigma-Aldrich. Sodium citrate (enzyme grade) was purchased from Fisher Scientific. They were used without further purification. Milli-Q water was filtered by Quantum Ex, Ultrapure Oranex Cartridge (Millipore) filtration columns and used for all experiments. All glassware were cleaned overnight in the mixture solution prepared by dissolving 120 g of Nochromix (Godax Laboratories, Inc.) powder in 3.78 L of concentrated sulfuric acid and were then thoroughly rinsed with Milli-Q water. Standard polyimide-coated fused silica single-hole capillary, outer diameter (OD) = 850 μm and inner diameter (ID) = 700 μm, were purchased from Polymicro Technologies. Borosilicate glass multihole capillary preform that has 2700 uniform hexagonal holes with a hole size of 17.7 μm was obtained from Incom, Inc.

Synthesis of Au-NPs. Au-NPs were synthesized using the UV-assisted photochemical method as described in the previous report.[8] Briefly, to achieve Au-NPs that have an average size of 117 ± 20 nm in diameter, a molar ratio of 1:1.7 for $HAuCl_4$ and sodium citrate were stirred for ∼2 min and then placed under a UV lamp (Dymax 2000-EC UV curing light source flood lamp system). The sample was then stirred continuously for 10 min until the color of the solution changed from yellow to reddish or orange.

Fabrication of SERS-Active Single- and Multihole Capillaries. Microstructured multihole capillaries were fabricated using an in-house computer-controlled fiber/capillary drawing system and the multihole capillary preform. To keep a certain air pressure inside the channels, a piece of 5 cm long preform was used and sealed at both ends using glue. The preform was pulled to achieve a desired inner diameter by optimizing the heating time, and feeding and pulling speeds.

In the experiments, four different structures were investigated, including single-hole capillary without polyimide coating (ID = 700 μm) (considered a 2-D structure with a flow channel), multihole capillary preform (ID = 17.7 μm), and two pulled multihole capillaries (ID = 7.5 and 4.7 μm, respectively). To achieve a clean surface before PAH modification, all the structures were illuminated under UV light for 1 h, then cleaned with ethanol under ultrasound for 30 min, and finally illuminated under UV light for another 1 h.

After the treatment, the single- and multihole capillaries were further modified with PAH, which provides anchoring sites for Au-NPs. The Au-NP surface coverage density can be controlled by changing the pH, concentration of PAH solution,[22] and/or Au-NP immobilization time.[8] To obtain similar Au-NP surface coverage density, the single-hole capillary and the other three multihole capillaries with the same length (e.g., 5 mm) were assembled into flat-end needles, and flowed with 0.2 and 0.05 mg/mL PAH in water solution of pH 5 for 20 min, respectively. Then Mill-Q water was continuously flowed to remove completely unbound and/or weakly adsorbed PAH molecules from the capillaries. Finally, ∼117 nm Au-NP with a concentration of $\sim 2.4 \times 10^{10}$ particles/mL was delivered into the single-hole capillary for 30 min and the multihole capillaries for 5 min, respectively.

Au-NP Surface Coverage Density Analysis. Au-NP immobilized capillaries were characterized using high-resolution scanning electron microscopy (SEM) (Philips XL30FEG) with a working distance of between 7 and 8 mm, a spot size of 2, and an accelerating voltage of 25 kV. The images (100 000× magnification) were captured using a backscattered electron detector and analyzed with ImageJ analysis software. The average coverage and standard deviation data were obtained from SEM images of five different locations on each capillary.

Raman and SERS Measurements. Raman and SERS measurements were carried out with the custom-built Raman spectroscopy system, consisting of a 785 nm excitation laser (Process Instruments PI-ECL-785-300-FC-SH) and a spectrometer (Horiba Scientific iHR550) equipped with a 600 grooves/mm grating and a spectroscopy-grade CCD. In this system, the laser beam was focused using an aspheric lens (N.A. = 0.25 and f = 11 mm) with 12 mW of optical power. The same aspheric lens was used for excitation of the laser and collection of the Raman signal from capillaries in a transverse detection arrangement (i.e., laser excitation and Raman collection is perpendicular to capillaries). Raman data acquisition time of 2 s was used for all experiments.

RESULTS AND DISCUSSION

To realize the SERS-active structure, the first important step is Au-NP immobilization on the inner surface of the capillaries using a polymer-mediated self-assembly approach similar to that used in a previous work.[22] In this study, we used negatively charged citrate stabilized Au-NPs that were synthesized by the modified UV-assisted photochemical method as described previously.[8] Since these capillaries have negatively charged surfaces (Figure 1a), to attach negatively charged Au-NP, positively charged PAH was deposited on the capillary inner walls to provide anchoring sites for Au-NPs (Figure 1b). Subsequently, the Au-NPs were immobilized inside the channel (Figure 1c). In these experiments, we deliberately selected large Au-NPs (117 ± 20 nm), which have higher scattering efficiency and better SERS enhancement than smaller ones.[8]

To investigate the SERS performance of these capillaries in vapor detection, we chose two model vapors: pyridine with high vapor pressure and 4-nitrophenol with low vapor pressure, both of which are commonly seen hazardous chemicals.[23,24] In the experiments, the Au-NP immobilized capillaries were first placed 1 cm above the analytes in open air at room temperature and then the vapor was drawn using either syringe or

dx.doi.org/10.1021/ac300175v | Anal. Chem. 2012, 84, 3376−3381

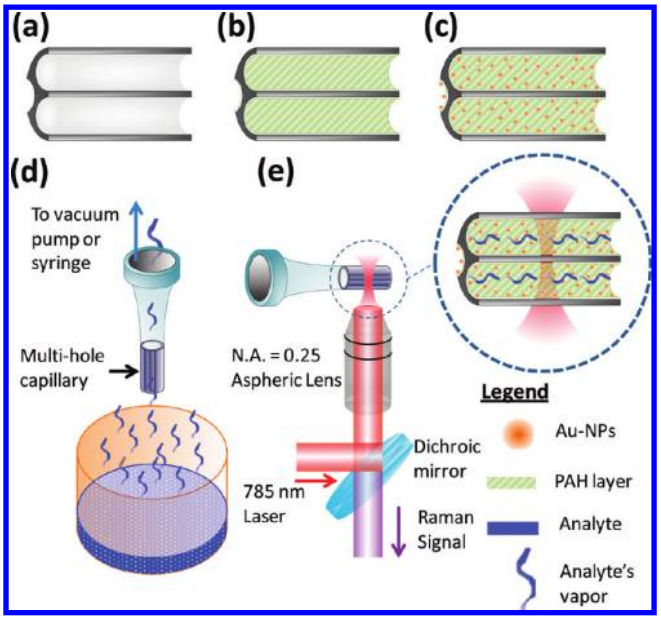

Figure 1. Schematic of SERS-active multihole capillary fabrication and vapor detection: (a) a cross section of bare multihole capillary, (b) PAH modification of the inner surface of the capillary, (c) Au-NP immobilization, (d) capturing vapor sample assisted by a mini diaphragm pump or a syringe, and (e) acquiring Raman signal with customized Raman system.

minipump for sampling (Figure 1d). In the case of pyridine, a syringe was used to suck the vapor. Pyridine is a highly volatile molecule with a very high vapor pressure (20 mmHg) at room temperature,[25] and the corresponding concentration in air under saturation conditions is 26 315 ppm. For 4-nitrophenol vapor detection, a mini diaphragm vacuum pump (Parker D713-22-01) was used to deliver the vapor into the capillaries. The vapor pressure of 4-nitrophenol at room temperature is only 1.9×10^{-5} mmHg,[26] corresponding to a vapor concentration of 19 ppb under saturation conditions. After vapor sampling, the capillaries were immediately interrogated using a customized Raman spectroscopy system (Figure 1e).

To assess the ID-dependent SERS performance of multihole capillaries, three different sizes of multihole capillaries (ID = 4.7, 7.5, and 17.7 μm) were chosen as shown in parts (a) and (d) of Figure 2, (b) and (e) of Figure 2, and (c) and (f) of Figure 2, respectively. A single-hole capillary (ID = 700 μm) was employed as a control. Figure 2g–i show the SEM images of the Au-NP immobilized on the inner surface of the multihole capillaries, showing discrete and uniform distribution of Au-NPs. Au-NP density was 4.24 ± 0.65, 4.58 ± 0.72, 2.51 ± 0.65, and 4.12 ± 0.98 particles/μm^2 for 4.7, 7.5, and 17.7 μm multihole capillaries and 700 μm single-hole capillary, respectively.

The SERS spectra for pyridine and 4-nitrophenol from four different capillaries at saturation vapor concentration are shown in Figure 3a,b. In pyridine spectra, two major peaks of 1021 and 1045 cm^{-1} of symmetric and asymmetric ring breathing modes were observed,[27] which slightly shifted from 988 and 1027 cm^{-1}, respectively, based on the normal Raman measurement with pyridine liquid (see Figure S1a and Table S1). In 4-nitrophenol spectra, three main peaks, 869, 1120, and 1341 cm^{-1}, were observed, corresponding to C–H out-of-plane bending mode, C–H in-plane bending mode, and NO_2

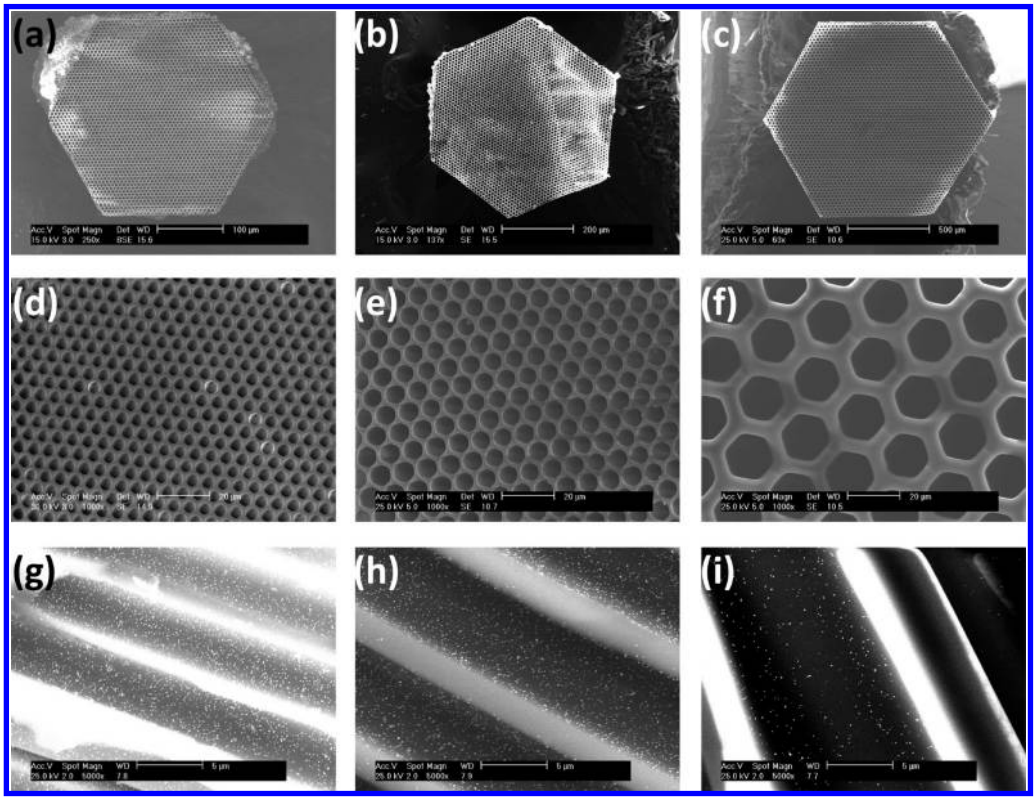

Figure 2. Scanning electron micrograph (SEM) images of the multihole capillaries with outer diameter of (a) 0.29 mm, (b) 0.59 mm, and (c) 1.42 mm whose individual capillary has inner diameter of (d) 4.7 μm, (e) 7.5 μm, and (f) 17.7 μm, respectively. SEM images of their cross sections along the channels with immobilized Au-NPs are in (g)–(i), respectively.

dx.doi.org/10.1021/ac300175v | *Anal. Chem.* 2012, 84, 3376–3381

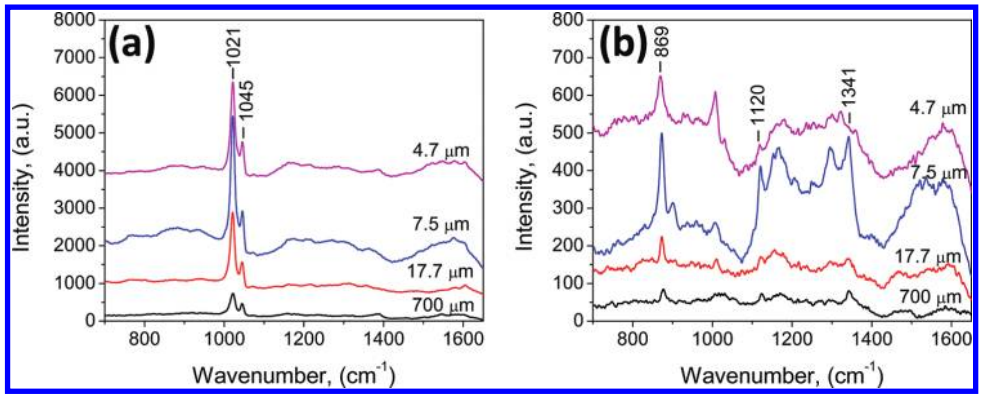

Figure 3. Surface-enhanced Raman spectra of (a) pyridine vapor and (b) 4-nitrophenol vapor detected using different sizes of capillaries. The curves are offset for clarity. The Raman measurements were done at 785 nm, 12 mW laser power, and acquisition time of 2 s. The vapor sampling was done at room temperature open space.

asymmetric stretching mode.[28] They also slightly shifted from 880, 1121, and 1335 cm^{-1} with respect to the normal Raman measurement (see Figure S1b and Table S2). These small differences of characteristic peaks between SERS and normal Raman are expected, as the interaction between the molecules and Au-NPs results in conformational changes in molecular vibration modes.[29,30]

The advantage of using 3-D multihole capillaries in the SERS vapor detection can be clearly seen when we compare with the SERS active area of a 2-D single-hole capillary. By analyzing the focal point image in Figure S2, we estimated that within the focal volume the ratio of the SERS active surface area was 17.4:26.9:20.8:1.0 for 4.7, 7.5, and 17.7 μm multihole capillaries and 700 μm single-hole capillary, respectively (Table 1). The

Table 1. Comparison among the Single-Hole Capillary and Three Different Sizes of Multihole Capillaries[a]

description	capillary with 4.7 μm holes	capillary with 7.5 μm holes	capillary with 17.7 μm holes	capillary with a 700 μm hole
surface area within focal volume	17.4	26.9	20.8	1
no. of Au-NP within focal volume	17.9	29.7	12.7	1
pyridine SERS intensity	4.3	6.1	3.4	1
4-nitrophenol SERS intensity	3.1	6.1	2.0	1

[a]Data are normalized to those of the 700 μm single-hole capillary.

corresponding ratio of the total number of Au-NPs was 17.9:29.7:12.7:1.0, respectively (Table 1). Considering the total SERS intensity is directly proportional to the total number of nanoparticles within the focal volume,[31] the 3-D multihole capillary would expect to yield over 1 order of magnitude increase in the SERS intensity, as compared to the 2-D single-hole capillary. Experimentally, the intensity ratios of four different capillaries (4.7, 7.5, 17.7, and 700 μm) are 4.3:6.1:3.4:1.0 and 3.1:6.1:2.0:1.0 for pyridine and 4-nitrophenol, respectively (Table 1). Note that both SERS intensity ratios for pyridine and 4-nitrophenol are similar and independent of type of gas molecules, which verifies that the SERS intensity depends on the total number of Au-NPs interacting with gas molecules within the focal volume.

However, the experimentally observed SERS intensity increase resulting from the multihole capillary (rows 3 and 4 in Table 1) is consistently 4−5 times lower than the corresponding theoretically estimated values (row 2 in Table 1). These differences are attributable to two possible reasons: (1) Au-NPs induced scattering and absorption losses along the focal penetration depth; thus, the multihole capillaries with a larger number of Au-NPs experienced more losses than the single-hole capillary. (2) Multiple layers of glass walls of multihole capillary introduced more scattering, reflection, and diffused wave, guiding losses along the capillary. Nevertheless, despite those degrading effects, the multihole capillary has achieved 2 to >6 times higher intensity (hence, signal-to-noise ratio) than the single-hole capillary experimentally.

With the inherent flow-through channels of the capillaries, we were able to investigate the adsorption kinetics of pyridine and 4-nitrophenol. Investigation of the kinetics of adsorption isotherm is important for predicting a concentration and reorganizing nature of molecular interaction. The SERS intensities of 1021 and 869 cm^{-1} were used to evaluate the adsorption kinetics of pyridine and 4-nitrophenol, respectively. The curves of high vapor pressure pyridine in Figure 4a are similar to those of the type I isotherm (usually termed as the Langmuir type, according to the International Union of Pure and Applied Chemistry (IUPAC) isotherm classification system[32]). The initial rapidly increasing SERS signal is due to the strong nonspecific interaction between the pyridine molecule and the SESR substrate. Pyridine adsorption reached the saturation level within approximately 5 s of flow into the capillaries regardless of capillary sizes (see insert in Figure 4a), indicative of the formation of a monolayer on the Au-NP surface. No further increase in the signal was observed beyond the plateau of the curve, as the weak attraction among pyridine molecules prevents them forming an additional layer.

In contrast, adsorption isotherm curves of low vapor pressure 4-nitrophenol in Figure 4b are different from those of pyridine. They resemble IUPAC standard type V adsorption isotherm.[32] The initial SERS signal was very low (was not observable until after a certain period) and then it slowly increased and reached the saturation level. This behavior can be accounted for by the weak interaction between 4-nitrophenol molecule and the SERS substrate, but the strong interaction among 4-nitrophenol molecules themselves. Therefore, the uptake of 4-nitrophenol on the SERS substrate is initially slow until the surface coverage is sufficient. Then the strong interaction between adsorbed and

dx.doi.org/10.1021/ac300175v | Anal. Chem. 2012, 84, 3376−3381

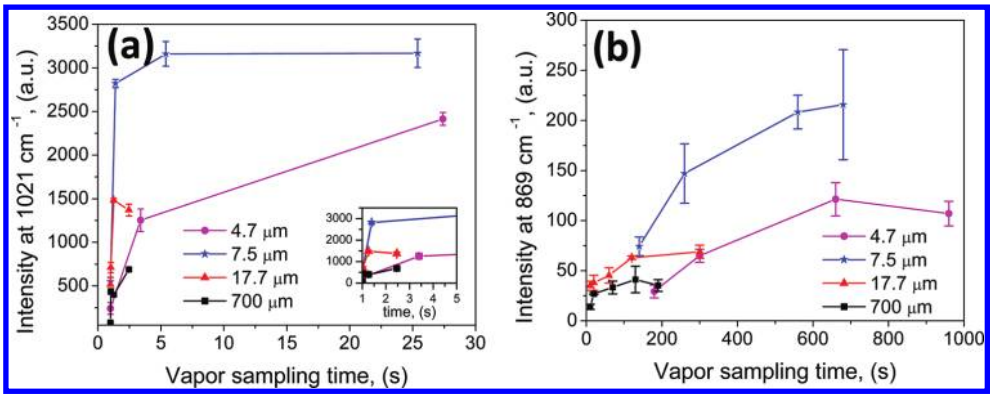

Figure 4. (a) SERS intensity at 1021 cm^{-1} (symmetric ring breathing mode) of pyridine and (b) SERS intensity at 869 cm^{-1} (C−H out-of-plane bending mode) of 4-nitrophenol varies with vapor pumping time at room temperature open space using different sizes of capillaries [ID = 4.7 μm (pink circle), 7.5 μm (blue star), 17.7 μm (red triangle), and 700 μm (black square)]. Insert: Enlarged portion of pyridine detection during the first 5 s. Error bars were obtained from three sets of each capillary. The Raman measurements were done at 785 nm, 12 mW laser power, and acquisition time of 2 s.

free 4-nitophenol molecules begins to dominate the adsorption process, resulting in further increase in the SERS signal. Note that in Figure 4b the required time to achieve the saturation level varies for different sizes of capillaries. For both 17.7 μm multihole and 700 μm single-hole capillaries, the 4-nitophenol SERS spectrum started to emerge around 10 s and reached the saturation level at about 100 s. However, much longer time, 600 s, was required to reach the saturation level for both 7.5 and 4.7 μm multihole capillaries. This phenomenon is simply due to the different flow rates for different sizes of capillaries, as exhibited in Figure S3. Using the adsorption isotherm curves in Figure 4, we are able to estimate the multihole capillary's sensing capability. For example, the saturation level achieved in the 7.5 μm multihole capillary is about 215 arbitrary units (a.u.) for 19 ppb 4-nitrophenol, which corresponds to a detection limit of 0.5 ppb (considering 3 standard deviation of the system noise as the minimum detectable signal).

CONCLUSIONS

We have developed a novel 3-D SERS platform using multihole capillaries immobilized with Au-NPs for rapid and ultrasensitive vapor detection. More than sixfold SERS enhancement was achieved using the multihole capillary in comparison with a similar 2-D structure. We further demonstrated rapid detection of pyridine vapor within 1 s of exposure and ultrasensitive detection of 4-nitropheol vapor within 10 s. A detection limit of 0.5 ppb for 4-nitropheol was achieved. As a result of their ultrasensitive capability, two different adsorption isotherm phenomena, type I and type V, were identified in pyridine and 4-nitrophenol detection, respectively. Therefore, this flow-through multihole capillary SERS platform exhibits great potential to enable many applications that require high sensitivity, real-time measurement, and system miniaturization.

ASSOCIATED CONTENT

Supporting Information

Mode field diameter and penetration depth of 785 nm laser excitation, normal Raman spectra and their vibrational mode assignments of pyridine and 4-nitrophnoel, and calculated and measured flow rates of multihole capillaries are presented. This material is available free of charge via the Internet at http://pubs.acs.org.

AUTHOR INFORMATION

Corresponding Author

*E-mail: xsfan@umich.edu.

Notes

The authors declare no competing financial interest.

ACKNOWLEDGMENTS

M.K.K.O. and Y.G. contributed equally to this work.

REFERENCES

(1) Vo-Dinh, T.; Stokes, D. L. *Appl. Spectrosc.* **1993**, *47* (10), 1728−1732.
(2) Taranenko, N.; Alarie, J.-P.; Stokes, D. L.; Vo-Dinh, T. *J. Raman Spectrosc.* **1996**, *27* (5), 379−384.
(3) Stokes, D. L.; Pal, A.; Anantha Narayanan, V.; Vo-Dinh, T. *Anal. Chim. Acta* **1999**, *399* (3), 265−274.
(4) Hill, W.; Wehling, B.; Klockow, D. *Appl. Spectrosc.* **1999**, *53* (5), 547−550.
(5) Biggs, K. B.; Camden, J. P.; Anker, J. N.; Duyne, R. P. V *J. Phys. Chem. A* **2009**, *113* (16), 4581−4586.
(6) Rae, S. I.; Khan, I. *Analyst* **2010**, *135* (6), 1365−1369.
(7) Sylvia, J. M.; Janni, J. A.; Klein, J. D.; Spencer, K. M. *Anal. Chem.* **2000**, *72* (23), 5834−5840.
(8) Khaing Oo, M. K.; Chang, C.-F.; Sun, Y.; Fan, X. *Analyst* **2011**, *136* (13), 2811−2817.
(9) Wang, J.; Yang, L.; Boriskina, S.; Yan, B.; Reinhard, B. M. *Anal. Chem.* **2011**, *83* (6), 2243−2249.
(10) Nie, S.; Emory, S. R. *Science* **1997**, *275* (5303), 1102−1106.
(11) Kneipp, K.; Wang, Y.; Kneipp, H.; Perelman, L. T.; Itzkan, I.; Dasari, R. R.; Feld, M. S. *Phys. Rev. Lett.* **1997**, *78* (9), 1667.
(12) Baker, G. A.; Moore, D. S. *Anal. Bioanal. Chem.* **2005**, *382* (8), 1751−1770.
(13) Dieringer, J. A.; Wustholz, K. L.; Masiello, D. J.; Camden, J. P.; Kleinman, S. L.; Schatz, G. C.; Van Duyne, R. P. *J. Am. Chem. Soc.* **2008**, *131* (2), 849−854.
(14) Orendorff, C. J.; Gearheart, L.; Jana, N. R.; Murphy, C. J. *Phys. Chem. Chem. Phys.* **2006**, *8* (1), 165−170.
(15) Zhou, H.; Qiu, C.; Yu, F.; Yang, H.; Chen, M.; Hu, L.; Sun, L. *J. Phys. Chem. C* **2011**, *115* (23), 11348−11354.
(16) Mandal, M.; Ranjan Jana, N.; Kundu, S.; Kumar Ghosh, S.; Panigrahi, M.; Pal, T. *J. Nanopart. Res.* **2004**, *6* (1), 53−61.
(17) Golightly, R. S.; Doering, W. E.; Natan, M. J. *ACS Nano* **2009**, *3* (10), 2859−2869.
(18) Halvorson, R. A.; Vikesland, P. J. *Environ. Sci. Technol.* **2010**, *44* (20), 7749−7755.
(19) Roth, E.; Kiefer, W. *Appl. Spectrosc.* **1994**, *48* (10), 1193−1195.

(20) Carron, K. T.; Kennedy, B. J. *Anal. Chem.* **1995**, *67*, 3353−3356.
(21) Heaps, D. A.; Griffiths, P. R. *Appl. Spectrosc.* **2005**, *59*, 1305−1309.
(22) Han, Y.; Tan, S.; Khaing Oo, M. K.; Pristinski, D.; Sukhishvili, S.; Du, H. *Adv. Mater.* **2010**, *22* (24), 2647−2651.
(23) Patnaik, P. Heterocyclic Compounds. In *A Comprehensive Guide to the Hazardous Properties of Chemical Substances*; John Wiley & Sons, Inc.: New York, 2006; pp 484−495.
(24) Patnaik, P. Phenols. In *A Comprehensive Guide to the Hazardous Properties of Chemical Substances*; John Wiley & Sons, Inc.: New York, 2006; pp 821−833.
(25) GSI Environmental Inc. 2211 Norfolk St. Suite 1000, Houston Texas 77098. http://www.gsi-net.com/en/publications/gsi-chemical-database/single/474 (accessed 03/15/2012).
(26) GSI Environmental Inc. 2211 Norfolk St. Suite 1000, Houston Texas 77098. http://www.gsi-net.com/en/publications/gsi-chemical-database/single/399.html (accessed 03/15/2012).
(27) Bilmes, S. A. *Chem. Phys. Lett.* **1990**, *171* (1−2), 141−146.
(28) Perry, D. A.; Son, H. J.; Cordova, J. S.; Smith, L. G.; Biris, A. S. *J. Colloid Interface Sci.* **2010**, *342* (2), 311−319.
(29) Tanaka, T.; Nakajima, A.; Watanabe, A.; Ohno, T.; Ozaki, Y. *Vib. Spectrosc.* **2004**, *34* (1), 157−167.
(30) Zuo, C.; Jagodzinski, P. W. *J. Phys. Chem. B* **2005**, *109* (5), 1788−1793.
(31) Kneipp, K.; Kneipp, H.; Kneipp, J. *Acc. Chem. Res.* **2006**, *39* (7), 443−450.
(32) Sing, K. S. W.; Everett, D. H.; Moscou, L.; Pierrotti, R.; Roquerol, J.; Siemeniewska, T. *Pure Appl. Chem.* **1985**, *57*, 603−619.